THE JOURNAL OF PHYSICAL CHEMISTRY C

C: Physical Processes in Nanomaterials and Nanostructures

Density, Structure, and Stability of Citrate and HCitrate on Bare and Coated Gold Nanoparticles

Gene Chong, Elizabeth D. Laudadio, Meng Wu, Catherine J. Murphy, Robert J Hamers, and Rigoberto Hernandez

J. Phys. Chem. C, **Just Accepted Manuscript** • Publication Date (Web): 19 Nov 2018

ACS Publications

is published by the American Chemical Society. 1155 Sixteenth Street N.W., Washington, DC 20036

Density, Structure, and Stability of Citrate^{3-} and H_2citrate$^-$ on Bare and Coated Gold Nanoparticles

Gene Chong[†], *Elizabeth D. Laudadio*[‡], *Meng Wu*[§], *Catherine J. Murphy*[§], *Robert J. Hamers*[‡], *Rigoberto Hernandez**[†]

[†] Department of Chemistry, Johns Hopkins University, Baltimore, Maryland 21218, United States

[‡] Department of Chemistry, University of Wisconsin—Madison, Madison, Wisconsin 53706, United States

[§] Department of Chemistry, University of Illinois at Urbana—Champaign, Urbana, Illinois 61801, United States

ABSTRACT

We simulate the packing of citrate^{3-} and H_2citrate$^-$ onto gold nanoparticles (AuNPs) to understand how citrate anions cap and stabilize AuNPs. We determine the molecular configurations of citrate on 4, 6, and 8 nm AuNP surfaces as a function of charge state and packing density and find that both the distribution of configurations and maximum packing density are independent of AuNP size. A combination of molecular dynamics simulations and *in situ* Fourier transform infrared spectroscopy (FTIR) is employed to compare the molecular configurations, stability, and density of citrate on 4 nm citrate-coated (cit-AuNPs) and within polycation-wrapped 4 nm cit-AuNPs. FTIR experiments indicate the presence of H_2citrate$^-$ within polycation-wrapped cit-AuNPs with coordination between the H_2citrate$^-$ layer and polycation layer in agreement with simulations. Intermolecular hydrogen bonding between terminal carboxylic-acid groups of H_2citrate$^-$ stabilizes the anionic layer at the interface between cit-AuNPs and adsorbing charged molecules. The calculated total density of H_2citrate$^-$ on AuNPs decreases from 3.3×10^{-10} mol/cm^2 to 3.0×10^{-10} mol/cm^2 upon adsorption of a polycation due to some displacement of dangling H_2citrate$^-$ hydrogen bonded to the surface-bound layer. The density of the surface-bound layer is consistently 2.8×10^{-10} mol/cm^2 with and without polycation adsorption. We provide all-atom level insight into the distribution and organization of experimentally derived binding modes of citrate on bare and coated cit-AuNPs. The citrate density and surface charge density are determined for all-atom and coarse-grained modeling of cit-AuNPs, their functionalization, and transformations in complex environments.

1. Introduction

Citrate anions act as both reducing and capping agents in the synthesis of gold nanoparticles (AuNPs) through the Turkevich method.[1-2] They consequently make up the first natural layer coating engineered AuNPs. Once synthesized, AuNPs can be functionalized for use in biomedical applications, such as molecular sensing, drug delivery, and photothermal therapy.[3-4] In this latter process, the citrate layer must be readily displaced for the thiol functionalization[5-7] of AuNPs via citrate-thiol ligand exchange, and must also be stably adsorbed on the AuNP surface as the initial charged layer for layer-by-layer polyelectrolyte assembly.[8-10] An accurate characterization of citrate anions on the AuNP surface is, therefore, essential to characterize the structural and dynamic properties of the functionalized layer in the presence of citrate, and thereby the transformations of these functionalized AuNPs in biological environments that might promote or impede their intended function.[11-12]

The charge state, ligand density, structure, and stability of citrate on the AuNP surface are key measurables that influence AuNP functionalization though the correlations between them have not yet been fully resolved in the literature. Characterization of citrate-coated AuNPs (cit-AuNPs) has, thus far, focused on experimental techniques that require dried samples[13-16] and *in vacuo* density functional theory (DFT) calculations.[16] Further, computational characterization has largely focused on minimum-energy binding of a single $citrate^{3-}$ or $H_2citrate^{-}$ anion to a metal-nanoparticle surface[16-19] and reactive simulations limited to small time- and length-scales.[20] Using attenuated total reflectance-Fourier transform infrared spectroscopy (ATR-FTIR), characteristic peaks of hydrogen-bonded carboxylic acid groups were detected after sealing and isolating the citrate layer with long-chain alkanethiol functionalization, suggesting that citrate exists in the $H_2citrate^{-}$ state on the AuNP surface.[14] These ATR-FTIR studies further suggest the dominant citrate species as that involving the coordination of citrate to the AuNP surface via the central carboxylate group with terminal carboxylate groups also near the surface to promote intermolecular hydrogen bonding. Several possible relative orientations of the carboxylate groups to the AuNP surface are shown in Figure 1B, and the chemical structure of $H_2citrate^{-}$ is included in Figure S1 in the Supporting Information. The central carboxylate group is directly connected to the -C–OH group, while the terminal carboxylate groups are each separated from the -C–OH group by a $-CH_2$ group. The previous ATR-FTIR studies cited above also indicate the presence of a second dangling layer of $H_2citrate^{-}$, forming bilayered $H_2citrate^{-}$ complexes on the AuNP surface with an ideal organization of two surface-bound $H_2citrate^{-}$ hydrogen-bonded to one dangling $H_2citrate^{-}$. To understand the binding modes of citrate, peaks from ^{13}C solid-state nuclear magnetic resonance

(SSNMR) spectra of cit-AuNPs synthesized under varying initial citrate:Au molar ratios were assigned to molecular configurations of citrate^{3-} extrapolated from DFT calculations of fully deprotonated acetate, succinate, and glutarate anions on gold surfaces.[16] These studies show that the binding of both terminal carboxylate groups to the AuNP surface with central carboxylate and hydroxyl groups free is preferred at low packing density and that the binding of a single terminal carboxylate group to the AuNP surface is preferred at high packing density.

In addition to the wide variation in the reported charge states of citrate on the AuNP surface in the literature, the surface citrate density has also been seen to range widely from 2.8×10^{-10} mol/cm^2 to 7.8×10^{-10} mol/cm^2.[9,13-14] We use these units to be consistent with the reported literature, and note that they translate to the range of 1.7 molecules/nm^2 to 4.7 molecules/nm^2 in terms of natural units at the nanoparticle scale. The range for surface charge density widens, starting from 2.8×10^{-10} mol e/cm^2 up to 2.34×10^{-9} mol e/cm^2, if the charge state of citrate can include either H_2citrate$^-$ or citrate^{3-} on the AuNP surface. Several factors contribute to this broad range for ligand density. To approximate the surface citrate density, a geometric calculation[14] was performed by Park and Shumaker-Parry assuming that each adsorbed citrate has a rectangular covering of the surface with an area approximately equal to 28 Å^2. Their calculation underestimates the ligand density because it assumes that citrate anions adsorb along the length of the molecule with the central carboxylate group bound and terminal carboxylic-acid groups near the surface and does not consider other binding modes[16] of citrate. Elemental analysis of carbon[13] in cit-AuNPs has previously been used to determine citrate density, but this method also samples oxidized byproducts of citrate on AuNPs, overestimating the ligand density. Another factor that can lead to overestimates in the experimentally-determined ligand density arises from the drying process for preparing samples in both elemental analysis and ligand-density analysis by X-ray photoelectron spectroscopy (XPS)[9,15] as it leads to aggregation of ligands. Although AuNP shape, size, and effective surface charge are routinely reported in the characterization of engineered AuNPs,[21] reports on experimentally-determined ligand densities are less common; for citrate, such values not only range widely but are also limited. This is largely in part because citrate anions are present at high concentrations in solution, making it difficult to characterize and isolate the citrate anions on the AuNP surface *in situ* from those in the bulk solution, and are assumed to be readily displaced[7] upon functionalization of AuNPs. Most prior experiments have centered on the effective negative surface charge of cit-AuNPs and its effect on the acquisition of electropositive protein coronas[22-25] and cytotoxicity.[9-10] Generally, cationic AuNPs are considered more toxic than anionic AuNPs.[26-27] Beyond general toxicity, attention is increasingly being brought to molecular-level mechanistic understanding of how exposure to different ligand types with the same effective charge, such as citrate and anionic thiols and polyanions with varying hydrophobicity, elicits different gene-expression levels and other biological responses,[9-10,12,28-31] emphasizing the need, addressed here, for an accurate characterization of the structure and density of the citrate layer on AuNPs.

Several computational approaches have been used to model functionalization and biomolecular corona formation on cit-AuNPs and the nano-bio interface more generally.[32-33] In all-atom molecular dynamics simulations of polycation functionalization onto cit-AuNPs, citrate^{3-} molecules were explicitly modeled and fixed at a density of 2.8×10^{-10} mol/cm^2 on the AuNP surface.[34] In similar coarse-grained simulations, surface gold atoms were negatively charged to represent the citrate layer, and to construct the polycation-coated AuNP and investigate lipid self-assembly on such AuNPs.[35] Three possible models[36-37] for fibrillogenic-protein binding to cit-AuNPs have been reported recently. In one study,[36] the AuNP surface was homogeneously coated with citrate molecules at a density of 4.4 $\times$ 10^{-10} mol/cm^2, and only 10% of the molecules were charged as citrate^{3-} with 90% left neutral to account for local pH effects. In the other study,[37] both an all-atom and a coarse-grained point-charge model were used. For the all-atom model, surface gold atoms were positively charged to promote adsorption of citrate^{3-} at a surface density of 2.8 $\times$ 10^{-10} mol/cm^2 with a surface charge density of 8.4 $\times$ 10^{-10} mol e/cm^2. For the coarse-grained model, point charges were homogeneously distributed on a spherical NP, following the same surface charge density used in the all-atom model. Fixed point-charge coated nanoparticle models with varying surface charge density have also been used for top-down coarse-grained simulations of nanoparticle-membrane interfaces,[38-40] but experimental validation and bottom-up coarse-graining approaches are needed to predict reliably the biological outcomes of nanoparticle exposure.[32,41] In all cases, citrate molecules are explicitly modeled as an all-atom citrate^{3-}, or implicitly (in coarse-grained models) through a surface charge density on the order of what would be a high density of citrate^{3-} on the AuNP surface. These simulations assume that the density of citrate on the AuNP surface is constant and uniformly distributed in a monolayer and that citrate^{3-} molecules stay fixed on the surface at charged nano-bio interfaces. Recent simulation studies by other groups have investigated citrate adsorption onto gold surfaces to reveal face-dependent binding of citrate and its effects, such as in DNA adsorption onto cit-AuNPs,[42] and have determined the structure of citrate adlayers at a range of surface citrate densities ranging from 1.49 to 2.98 mol $\times$ 10^{-10} per cm^2 of an Au(111) slab,[43] but to our knowledge only the citrate^{3-} state was considered.

We perform all-atom molecular dynamics simulations to investigate the density, structure, and stability of both citrate^{3-} and H_2citrate^{-} on AuNPs. We use implicit-solvent simulations to examine the maximum packing density and changes in the coordination modes of citrate^{3-} and

H_2citrate^{-} on the surface of 4, 6, and 8 nm AuNPs with increasing packing density. We find from implicit-solvent simulations that the maximum packing density and coordination modes of both citrate species on the AuNP surface are independent of nanoparticle size. Explicit-solvent simulations are used to determine if the structures of citrate^{3-} and H_2citrate^{-} layers on 4 nm AuNPs are consistent with those from implicit solvent. The coordination modes and spatial distribution for H_2citrate^{-} is independent of solvent condition but differ significantly for citrate^{3-} between implicit and explicit solvents. The coordination modes of citrate determined previously from ATR-FTIR[14] and ^{13}C SSNMR[16] experiments agree with those found for the H_2citrate^{-} state in our explicit-solvent simulations. Representative images of the coordination modes of citrate examined in this study and structures of 4 nm cit-AuNPs in implicit and explicit solvent are shown in Figure 1. Representative structures of 6 and 8 nm cit-AuNPs in implicit solvent are shown in the Supporting Information. These structures also qualitatively show face-dependent binding of citrate on metal nanoparticles, which has been shown for citrate and other ligands by experiment[14] and simulation.[18,44-47]

We test the stability of citrate^{3-} and H_2citrate^{-} layers by depositing a 200-mer polycation poly(allylamine hydrochloride), PAH_{200}, on cit-AuNPs. We find that PAH_{200} highly disrupts the citrate^{3-} layer on the AuNP surface. In contrast, PAH_{200} displaces the dangling H_2citrate^{-} layer, but there is no change in the density of the surface-bound H_2citrate^{-} layer. Representative structures of PAH-wrapped cit-AuNPs (PAH-cit-AuNPs) are shown in the Supporting Information. We use *in situ* ATR-FTIR on PAH-cit-AuNPs to show that citrate exists as H_2citrate^{-} at highly charged interfaces. The intermolecular hydrogen bonding between H_2citrate^{-} stabilizes the negatively charged layer in the presence of adsorbing positively charged molecules, such as PAH_{200}. The density of H_2citrate^{-} on AuNPs including the dangling H_2citrate^{-} layer totals 3.3×10^{-10} mol/cm^2

and is 2.8 × 10^{-10} mol/cm^2 for the surface-bound layer. The total density of H_2citrate$^-$ across the two layers decreases slightly to 3.0 × 10^{-10} mol/cm^2 upon adsorption of PAH_{200} due to some displacement of the dangling second H_2citrate$^-$ layer, and the density of the surface-bound H_2citrate$^-$ layer remains consistent. The surface charge density contributed by H_2citrate$^-$ directly on the AuNP surface is 2.8 × 10^{-10} mol *e*/cm^2 nonuniformly distributed due to face-dependent binding.

Through a combination of molecular dynamics simulations and *in situ* ATR-FTIR spectroscopy, we determine an ensemble of binding modes that collectively stabilize the citrate layer capping the metal nanoparticles on bare and polycation-coated AuNPs and ultimately determine its structure and density. We provide a consensus citrate density for the citrate^{3-} and H_2citrate$^-$ states to aid in the experimental characterization of as-synthesized and functionalized cit-AuNPs, a surface density of H_2citrate$^-$ that is appropriate for the implementation of all-atom and coarse-grained models, and a surface-charge density for fixed-charge coarse-grained models of cit-AuNPs.

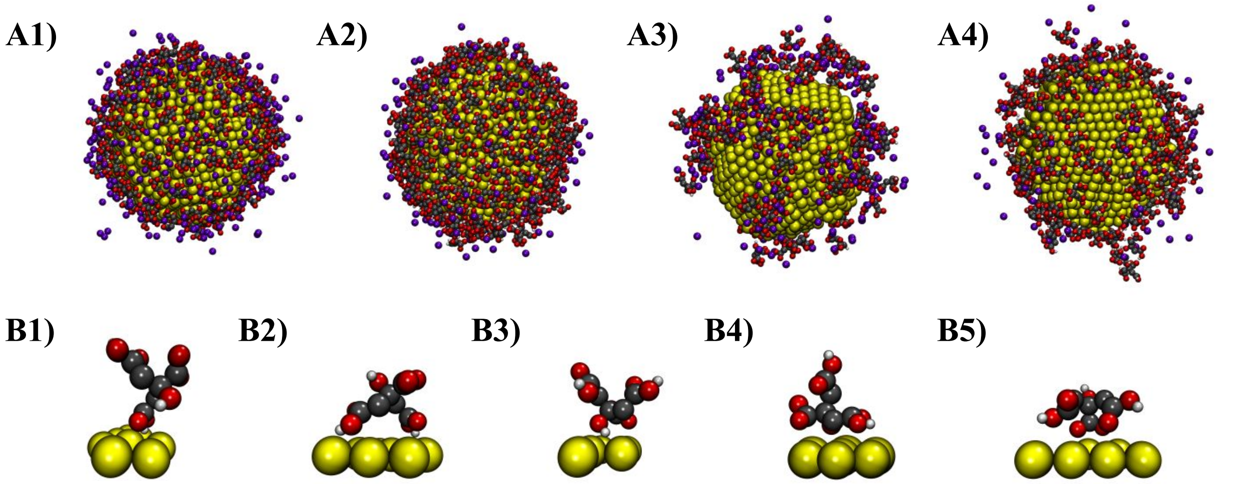

Figure 1. Representative 4 nm cit-AuNPs in row A (top), and citrate configurations in row B (bottom): (A1) Citrate^{3-} monolayer maximally packed on AuNPs in implicit solvent, (A2) H_2citrate^{-} monolayer maximally packed on AuNPs in implicit solvent, (A3) citrate^{3-} on AuNPs in explicit solvent, and (A4) H_2citrate^{-} on AuNPs in explicit solvent; (B1) Tall, (B2) bridge, (B3) 0-arm, (B4) 1-arm, and (B5) 2-arm citrate configurations on AuNPs described in this study. The "tall" configuration has a single terminal carboxylate group bound to the AuNP surface. The "bridge" configuration has both terminal carboxylate groups bound to the surface with the central carboxylate and hydroxyl groups free. The 0-, 1-, or 2-arm configurations have either the central carboxylate or hydroxyl group bound to the surface with 0, 1, or 2 terminal carboxylate groups also bound, respectively. Cit-AuNPs consist of gold (yellow), carbon (gray), oxygen (red), and hydrogen (white) atoms. Na^+ ions are shown in purple; water and counterions outside the solvent shell are removed for clarity in row A. Configurations are shown in the H_2citrate^{-} state in row B.

2. Methods

2.1. Molecular Dynamics Simulations. To simulate the packing of citrate, we applied a steering force of 0.1 kcal/(mol Å) on citrate anions toward the nanoparticle center until they were within 7.5 Å from either the bare nanoparticle surface or a monolayered citrate surface depending on the initial condition of the simulation. Beyond this cutoff distance, the steering force is no longer applied, and the citrate anions remain within the 10 Å cutoff for pairwise interactions such that citrate anions can weakly interact with and potentially adsorb to the gold surface. Steering forces in the range of 0.1-5.0 kcal/(mol Å) were initially tested (data not shown), and a weak steering force of 0.1 kcal/(mol Å) was chosen to ensure that citrate anions were dispersed in solvent without artificial jamming in the vicinity of the cutoff distance of the steering force. The steering force was not employed during equilibration, enabling desorption of excess citrate from the nanoparticle surface. All simulations were carried out using LAMMPS,[48] using periodic boundary conditions and a 1.0 fs timestep. Specific details on the simulation setup and force-field parameters are provided in the Supporting Information.

For implicit-solvent simulations, five simulations for the adsorption of citrate^{3-} and five for H_2citrate^{-} adsorption onto AuNPs were run for each AuNP size. The implicit solvent was modeled using Langevin dynamics at 300 K with a damping constant of 10 ps^{-1} and a dielectric constant of 80.1, with the particle-particle particle-mesh (PPPM) method used for long-ranged electrostatic calculations.

For explicit-solvent simulations, we ran five simulations each of the adsorption of citrate^{3-} and H_2citrate^{-} onto 4 nm AuNPs in TIP3P solvent and five simulations each of PAH_{200} deposition onto the equilibrated 4 nm AuNPs coated with citrate^{3-} and H_2citrate^{-} under constant *NPT* conditions —that is, for number of atoms N, pressure P at 1.0 atm, and temperature T at 300 K— using the PPPM method for long-ranged electrostatic calculations.

2.2. Cit-AuNP Synthesis. Cit-AuNPs of about 4 nm in diameter were synthesized by a flow reactor system according to the reported procedure.[49] In a typical synthesis, 1600 mL nanopure water and 20 mL of 0.01 M $HAuCl_4 \cdot 3H_2O$ were mixed in a 2 L Erlenmeyer flask and were wrapped with aluminum foil. Freshly prepared 10 mL 0.10 M $NaBH_4$ was added to ice-cold 1616 mL nanopure water in another 2 L Erlenmeyer flask. Both solutions were sent through a flow reactor with a peristaltic pump at a flow rate of 40 mL/min. Cit-AuNP dispersion was orange in color and had a concentration of about 4 nM (of particles).

2.3. PAH-Cit-AuNP Synthesis. 32 mL of 100 mM NaCl and 100 mL of PAH solution (Mw 17.5 kDa) (10 g/L in 1 mM NaCl) was added separately to the above synthesized cit-AuNP dispersion with vigorous stirring. Stirring continued overnight, and the nanoparticle dispersion was concentrated to 60 mL by diafiltration cassettes (Tangential flow filtration capsules, 50k MWCO, VWR). The concentrated nanoparticle dispersion was first filtered through a SFCA membrane filter (Syringe filter, 0.45 μm, Corning), then was purified by two rounds of centrifugal filtration (Ultra centrifugal filter, 10k MWCO, Amicon), and redispersed in nanopure water. Finally, particle dispersion was diluted to 10 mL after two rounds of centrifugal filtration. PAH-cit-AuNP dispersion was wine red in color and had a concentration of about 150 nM (of particles). Additional characterization of PAH-cit-AuNPs is provided in the Supporting Information.

2.4. ATR-FTIR Spectroscopy. ATR-FTIR spectra of PAH-cit-AuNPs were acquired using a Pike GladiATR attachment equipped with a triple-bounce diamond IRE on a Bruker Vertex 70 FTIR instrument. Each spectrum was acquired at a resolution of 4 cm^{-1} and signal-averaged over 500 scans. All absorbance spectra were taken in solution and are referenced to ultrapure water.

3. Results and Discussion

3.1. Maximum Packing Density of $Citrate^{3-}$ Monolayers, $H_2citrate^{-}$ Monolayers, and $H_2citrate^{-}$ Bilayers on 4, 6, and 8 nm AuNPs. To simulate the packing of citrate anions onto AuNPs using molecular dynamics simulations, we first randomly distributed 3 $citrate^{3-}$ or $H_2citrate^{-}$ molecules nm^{-2} (5×10^{-10} mol cm^{-2}) in a simulation box with a 4, 6, or 8 nm AuNP fixed at the center. A steering force toward the center of the AuNP was applied to citrate anions until the anions were 7.5 Å from the AuNP surface. This process was run for at least 10 ns until the AuNP surface was saturated with citrate (Figure 2). Simulations were run for an additional 10 ns without a steering force and with data collected during the last 5 ns to analyze the citrate anions that remain packed on the AuNP surface.

In implicit solvent, we find that $citrate^{3-}$ maximally packs into a monolayer and that the development of high surface charge density prevents bilayer formation. We used this distinction to calculate a minimum Au–O distance between surface gold atoms and oxygen atoms of citrate needed to consider a citrate anion as bound to the AuNP surface in our simulations. We find that the number of $citrate^{3-}$ attached to the AuNP surface as a function of Au–O distance saturates beyond an Au–O distance of 3.5 Å, showing that this Au–O distance accounts for all $citrate^{3-}$ in the adsorbed monolayer (Figure S2 in Supporting Information). We, therefore, define the condition for which $citrate^{3-}$ or $H_2citrate^-$ being bound to the surface according to when the anion has an Au–O distance that is less than 3.5 Å.

The initial packing density of 3 molecules nm^{-2} corresponds to 150 citrates on a 4 nm AuNP, 340 citrates on a 6 nm AuNP, and 600 citrates on an 8 nm AuNP. The number of $citrate^{3-}$ attached after equilibration is lower than the initial packing density, whereas nearly all $H_2citrate^-$ adsorb onto the AuNP surface (Figure 2). The greater rate of $H_2citrate^-$ absorption and number of $H_2citrate^-$ adsorbed on AuNPs compared to $citrate^{3-}$ highlight the increased stability imparted to the anionic citrate layer by the intermolecular hydrogen bonding between $H_2citrate^-$ anions. We placed each of the equilibrated structures of AuNPs coated with $H_2citrate^-$ in a simulation box, to which we randomly distributed an additional 3 $H_2citrate^-$ molecules per nm^2 of gold surface. A steering force toward the center of the AuNP was applied to the newly added citrate anions until they were 15 Å from the AuNP surface. This process was run for 10 ns to promote $H_2citrate^-$ bilayer formation on the AuNPs. For calculations at the packing density of the dangling second layer in bilayered $H_2citrate^-$, any unbound molecule that has a maximum intermolecular O–H hydrogen-bonding distance within 4.0 Å with surface-bound $H_2citrate^-$ is considered to be in the second layer. The conservative choice of this cutoff distance is consistent with the maximum of the observed range of O–H bond distances.[50] Simulations were run without the steering force for 25 ns, and desorption of excess $H_2citrate^-$ was observed (Figure 3). The maximum packing density of each layer in bilayered $H_2citrate^-$ was determined from additional 5 ns production runs. Table 1 shows the increase in packing density from $citrate^{3-}$, to monolayered $H_2citrate^-$, and to bilayered $H_2citrate^-$ at 3.74, 5.67, and 8.42 $\times$ 10^{-10} mol/cm^2, respectively, for 4 nm AuNPs. The maximum packing density is largely consistent between 4, 6, and 8 nm AuNPs (Table 1). A slightly higher packing density for all citrate species on 4 nm AuNPs could be attributed to greater curvature of this AuNP surface relative to larger sized AuNPs. By dividing the maximum packing density of $H_2citrate^-$ in the surface-bound monolayer ($H_2citrate^-_{\text{Layer 1}}$) by that of $H_2citrate^-$ in the dangling, second layer ($H_2citrate^-_{\text{Layer 1+2}} - H_2citrate^-_{\text{Layer 1}}$) in Table 1, we determine a ratio of 2.06 for the number of $H_2citrate^-$ in the surface-bound layer to the number in the dangling second $H_2citrate^-$ layer on 4 nm AuNPs, 2.05 on 6 nm AuNPs, and 2.38 on 8 nm AuNPs. These values are close to the ideal distribution predicted by Park and Shumaker-Parry,[14] supporting the use of our simulation parameters and implicit-solvent model for the ideal, maximally packed $H_2citrate^-$-coated AuNPs. Our results suggest that the maximum citrate density reported in the literature[9] referenced in Table 1 can only be reached through some combination of bilayered $H_2citrate^-$ on the AuNP surface and aggregation of citrate anions upon drying of samples for characterization.

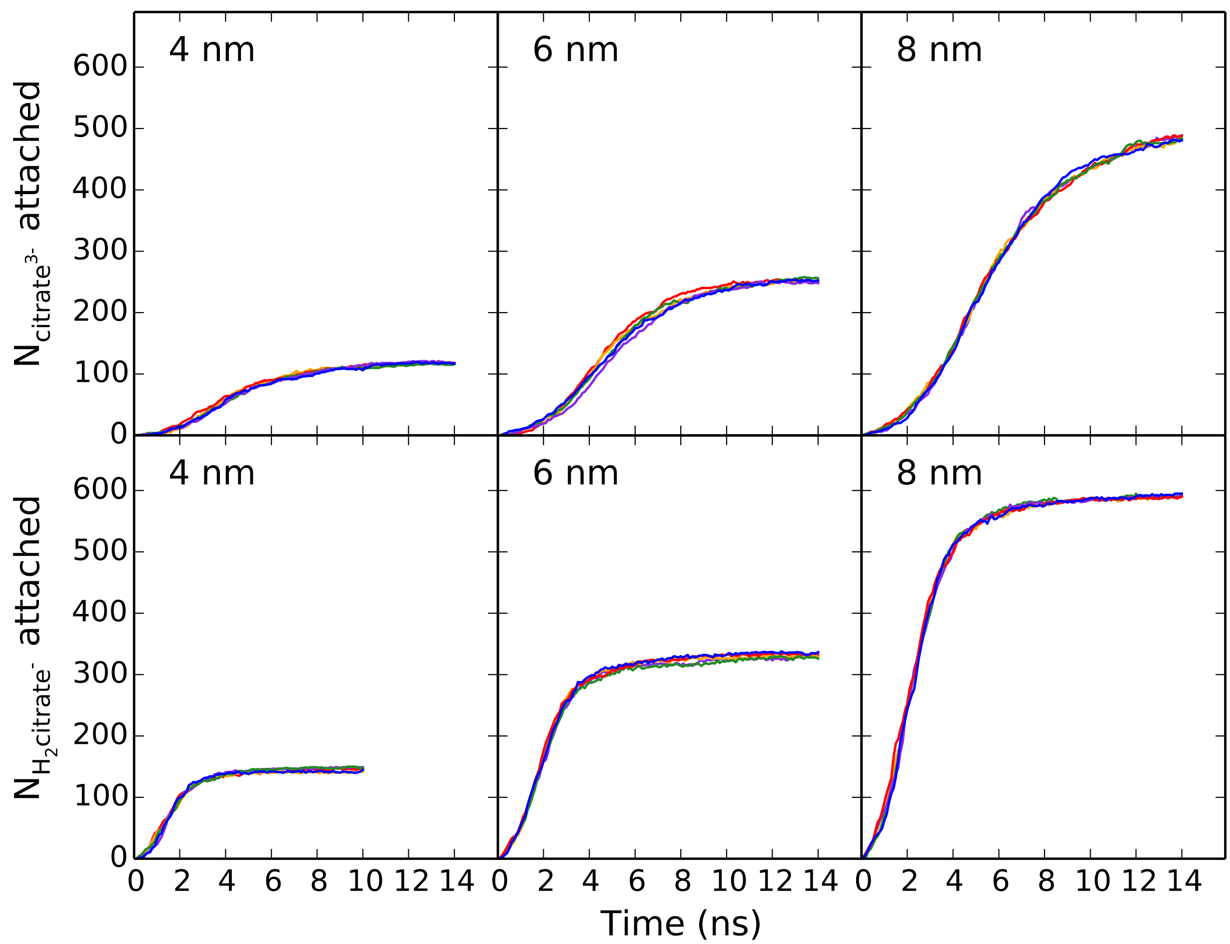

Figure 2. Number of citrate adsorbed onto 4, 6, and 8 nm AuNPs vs. time in implicit solvent, according to an Au–O cutoff distance of 3.5 Å and with an initial density of 3 citrate nm^{-2} randomly distributed in the simulation box. Trajectories are distinguished by color with no association between like colors in different panels.

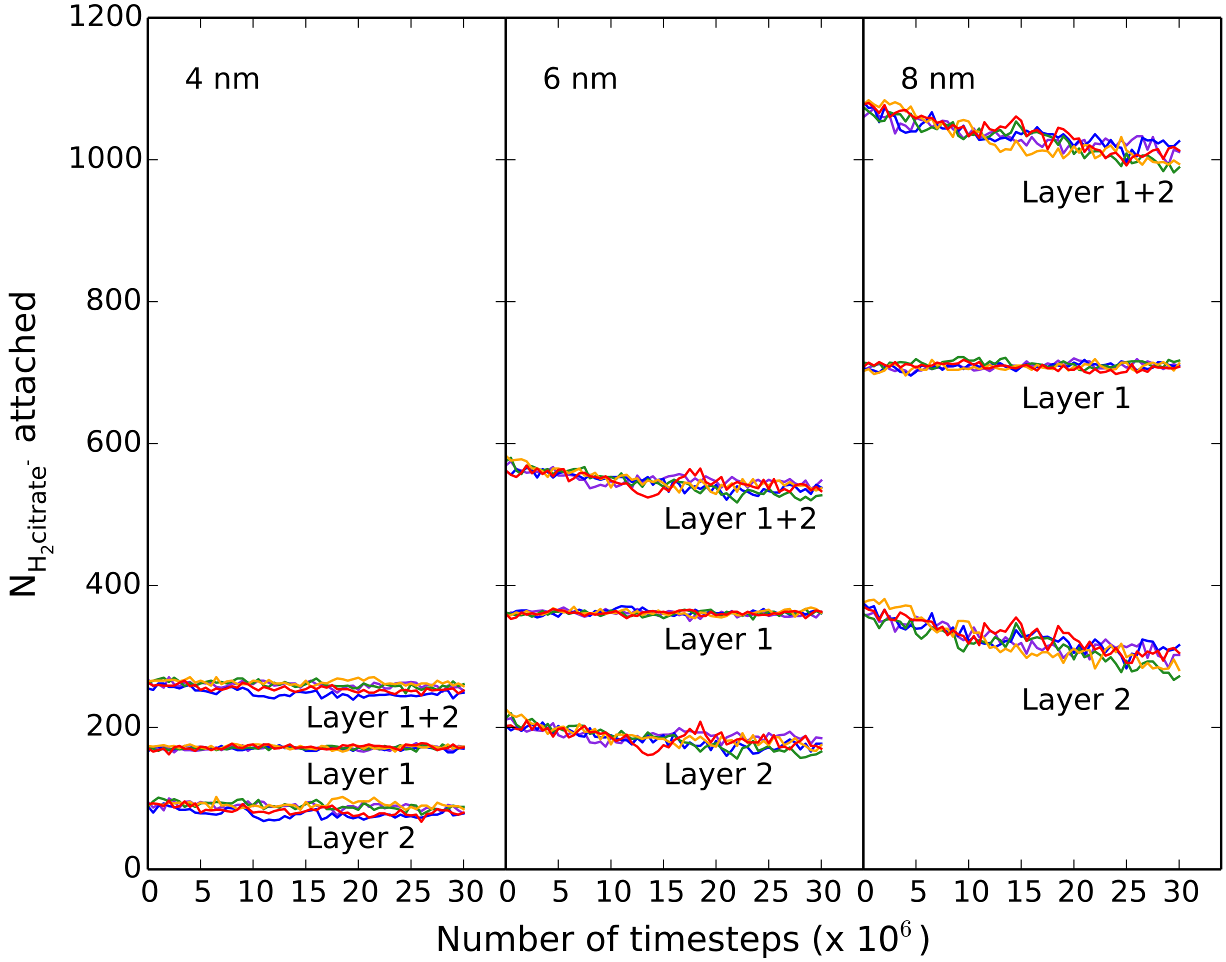

Figure 3. Number of H_2citrate$^-$ adsorbed onto 4, 6, and 8 nm AuNPs vs. time in implicit solvent with an additional density of 3 H_2citrate$^-$ nm^{-2} randomly distributed in the simulation box (totaling 6 H_2citrate$^-$ nm^{-2}) to saturate the surface-bound layer (Layer 1), promote the adsorption of a dangling second layer (Layer 2), and form bilayered H_2citrate$^-$ (Layer 1+2). Trajectories are distinguished by color with no association between like colors in different panels.

Table 1. Maximum packing densities of citrate^{3-}, H_2citrate$^-$ monolayers, and H_2citrate$^-$ bilayers compared to ligand densities calculated from experiment.

	Maximum packing density (mol cm^{-2} x 10^{-10}) Simulation			Experiment
	citrate^{3-}	H_2citrate$^-_{Layer\ 1}$	H_2citrate$^-_{Layer\ 1+2}$	
4 nm	3.74 ± 0.04	5.67±0.09	8.42±0.20	7.80[a]
6 nm	3.36 ± 0.03	4.97±0.05	7.39±0.10	
8 nm	3.48 ± 0.04	5.19±0.03	7.37±0.09	

[a]From reference[9]

3.2. Molecular Configurations of Citrate as a Function of AuNP Size and Packing Density. We used the Au–O cutoff distance of 3.5 Å to determine if each citrate is bound to the AuNP surface via the terminal carboxylate, central carboxylate, or hydroxyl group. We defined molecular configurations according to the groups bound to the surface (Figure 1B). The "tall" configuration is defined as a citrate that has an oxygen from a single terminal carboxylate group within the cutoff distance from the AuNP surface. The "bridge" configuration is distinguished by both terminal carboxylate groups of citrate bound to the surface with the central carboxylate and hydroxyl groups free. The configurations are considered 0-, 1-, or 2-arm if either the central carboxylate or hydroxyl group is bound to the surface with 0, 1, or 2 terminal carboxylate groups also bound, respectively.

Figure 4 shows the distribution of molecular configurations for surface-bound citrate anions on 4, 6, and 8 nm AuNPs. For monolayered $citrate^{3-}$, the dominant configurations are 1-arm and 2-arm, which combined make up ~78% of the configurations. Approximately 38-51% of monolayered $H_2citrate^{-}$ are in the 2-arm configuration across AuNP sizes, which is consistent with previous experimental findings by ATR-FTIR[14] that intermolecular hydrogen bonding between terminal carboxylic-acid groups of $H_2citrate^{-}$ stabilizes the citrate layer on AuNPs. The 1-arm and bridge configurations each make up ~21-26% of monolayered $H_2citrate^{-}$ configurations. We find that the bridge configuration, previously attributed to $citrate^{3-}$ at low packing density,[14] is significantly present in monolayered $H_2citrate^{-}$. For the surface-bound layer on an AuNP coated with a bilayer of $H_2citrate^{-}$ ($H_2citrate^{-}$, saturated), the percent distribution of 2-arm configurations decreases, accompanied by commensurate increases in the percent distribution of tall and bridge configurations. We find that the distribution of these configurations in monolayered $citrate^{3-}$, monolayered $H_2citrate^{-}$, and saturated $H_2citrate^{-}$ does not change with respect to AuNP size.

As the surface-bound H_2citrate$^-$ layer becomes saturated, the changes in molecular configurations reflect the need to maximize packing and promote bilayer formation. The bridge, 1-arm, and 2-arm configurations, each with at least one terminal carboxylic-acid group bound to the AuNP surface, stabilize monolayered H_2citrate$^-$. The bridge configuration maximizes packing compared to 2-arm, which can explain the increase in the percent distribution of the bridge configuration and decrease in the percent distribution of the 2-arm configuration in response to saturating the H_2citrate$^-$ layer. The percent distribution of the 1-arm configuration does not significantly change upon saturating the H_2citrate$^-$ layer. The 1-arm configuration maximizes packing and has one surface-bound and one free terminal carboxylic-acid group that can stabilize the surface-bound layer and promote bilayer formation, respectively. Lastly, there is a significant increase in the percent distribution of the tall configuration upon saturating the surface. The tall configuration has a free central carboxylate group and only one of the two terminal carboxylic-acid groups bound, maximizing packing on the AuNP surface. One of the two free groups in the tall configuration can potentially hydrogen bond with a free group from another tall configuration or the free central groups in the bridge configuration, while the remaining free group can hydrogen bond with a dangling citrate in the second layer. Such intermolecular interactions thereby maximize packing, stabilize the surface-bound layer, and promote bilayer formation, while maintaining the ideal 2:1 surface-bound to dangling citrate organization.

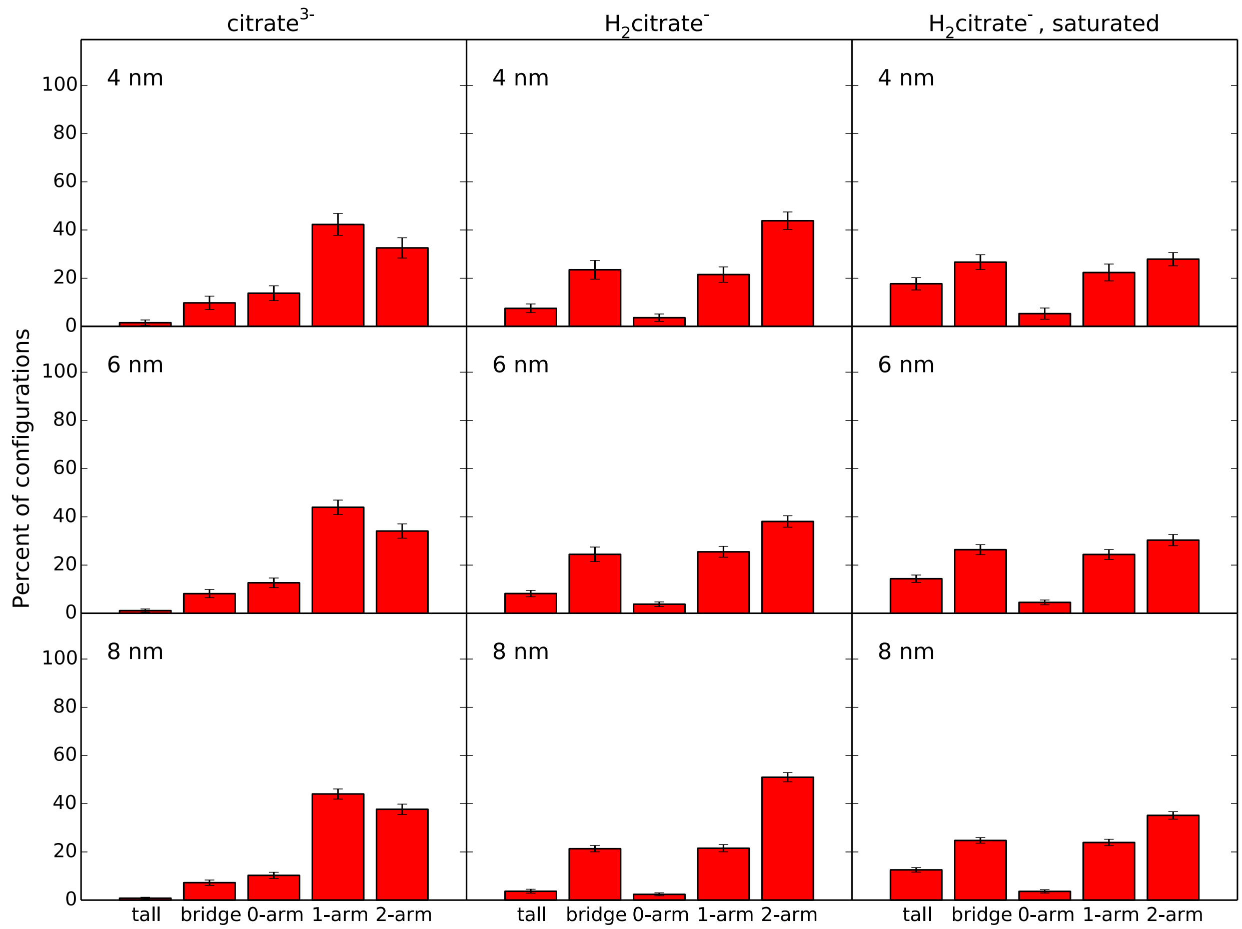

Figure 4. Distribution of molecular configurations in a monolayer of $citrate^{3-}$, monolayer of $H_2citrate^{-}$, and the saturated surface-bound layer of $H_2citrate^{-}$ within bilayered $H_2citrate^{-}$ on 4, 6, and 8 nm AuNPs in implicit solvent.

3.3. Density and Stability of $Citrate^{3-}$ and $H_2citrate^{-}$ on 4 nm Cit-AuNPs and PAH-Cit-AuNPs. We randomly distributed $citrate^{3-}$ and $H_2citrate^{-}$ equivalent to their maximum packing density on 4 nm AuNPs in a simulation box with the 4 nm AuNP fixed at the center. A steering force was applied on $citrate^{3-}$ and $H_2citrate^{-}$ onto 4 nm AuNPs in explicit TIP3P solvent at constant *NPT* until the anions were 7.5 Å from the AuNP surface for 20 ns. The citrate molecules were, then, kept frozen, and the solvent was equilibrated for 5 ns. The constraints on citrate were released, and the system was equilibrated for 10 ns. Lastly, a production run of 5 ns was performed with data collected at 10 ps intervals.

The polycation PAH_{200} was deposited on the equilibrated structures of cit-AuNPs along with desorbed excess citrate to test the stability of the citrate layers, and the system was re-solvated in TIP3P solvent (Figure 5). A steering force was applied to PAH_{200} toward the AuNP surface for 0.05 ns to promote adsorption of the polycation. The system was equilibrated for a total simulation time of 20 ns followed by a 5 ns production run. The numbers of adsorbed citrate molecules, following the construction and equilibration of cit- and PAH-cit-AuNPs, shown in Figs. 6 and 7, do not significantly change during the production runs.

In explicit solvent, we find that $citrate^{3-}$ molecules do not adsorb into a monolayer (Figures 1, 5, and S4 in Supporting Information). Rather, $citrate^{3-}$ anions coordinate with Na^+ ions and distribute radially from the AuNP surface due to the accumulation of high surface charge density on the AuNP surface in agreement with previous simulations.[43] Because $citrate^{3-}$ anions do not form a distinct monolayer in explicit solvent, we track the density and spatial distribution of $citrate^{3-}$ by distance from the AuNP surface in 3.5 Å increments. We calculate that approximately 28 $citrate^{3-}$ are directly bound to the surface of each AuNP (Figure 6). Beyond 17.5 Å, the number of $citrate^{3-}$ between increments does not significantly change, indicating that there is a total of approximately 82 $citrate^{3-}$ in the adsorbed layer and a surface charge density of 8.1×10^{-10} mol e/cm^2, distributed radially from face-dependent sites on the AuNP surface. The remaining $citrate^{3-}$ in the simulation box are free in solution. The difference in the number of $citrate^{3-}$ between increments signifies the number of $citrate^{3-}$ per layer. This spatial charge distribution changes upon adsorption of PAH (Figure 6). The intermolecular interaction between $citrate^{3-}$ through coordination with Na^+ ions becomes disrupted, and $citrate^{3-}$ detaches from the AuNP surface, preventing complete adsorption of PAH (Figure S4).

The density of H_2citrate$^-$ bilayers is determined by the 3.5 Å Au–O cutoff distance for the first layer and an intermolecular O–H distance within 4.0 Å between surface-bound and unbound H_2citrate$^-$ for the second layer. The density of H_2citrate$^-$ and surface charge density are 3.3×10^{-10} mol/cm^2 and 3.3×10^{-10} mol e/cm^2, respectively (Figure 7). We find that the dangling second layer of H_2citrate$^-$ is easily displaced by PAH, but the surface-bound layer is highly stable (Figure 7). The density of the surface-bound H_2citrate$^-$ layer remains fixed with a surface charge density of 2.8×10^{-10} mol e/cm^2, and the total surface charge density of the H_2citrate$^-$ bilayer is 3.0×10^{-10} mol e/cm^2 upon adsorption of PAH.

The stability of the H_2citrate$^-$ layer on AuNPs is in agreement with previous ATR-FTIR experiments, which found that the citrate layer on AuNPs is resistant to thiol functionalization,[4] and suggests that citrate anions are in the H_2citrate$^-$ state on AuNPs.

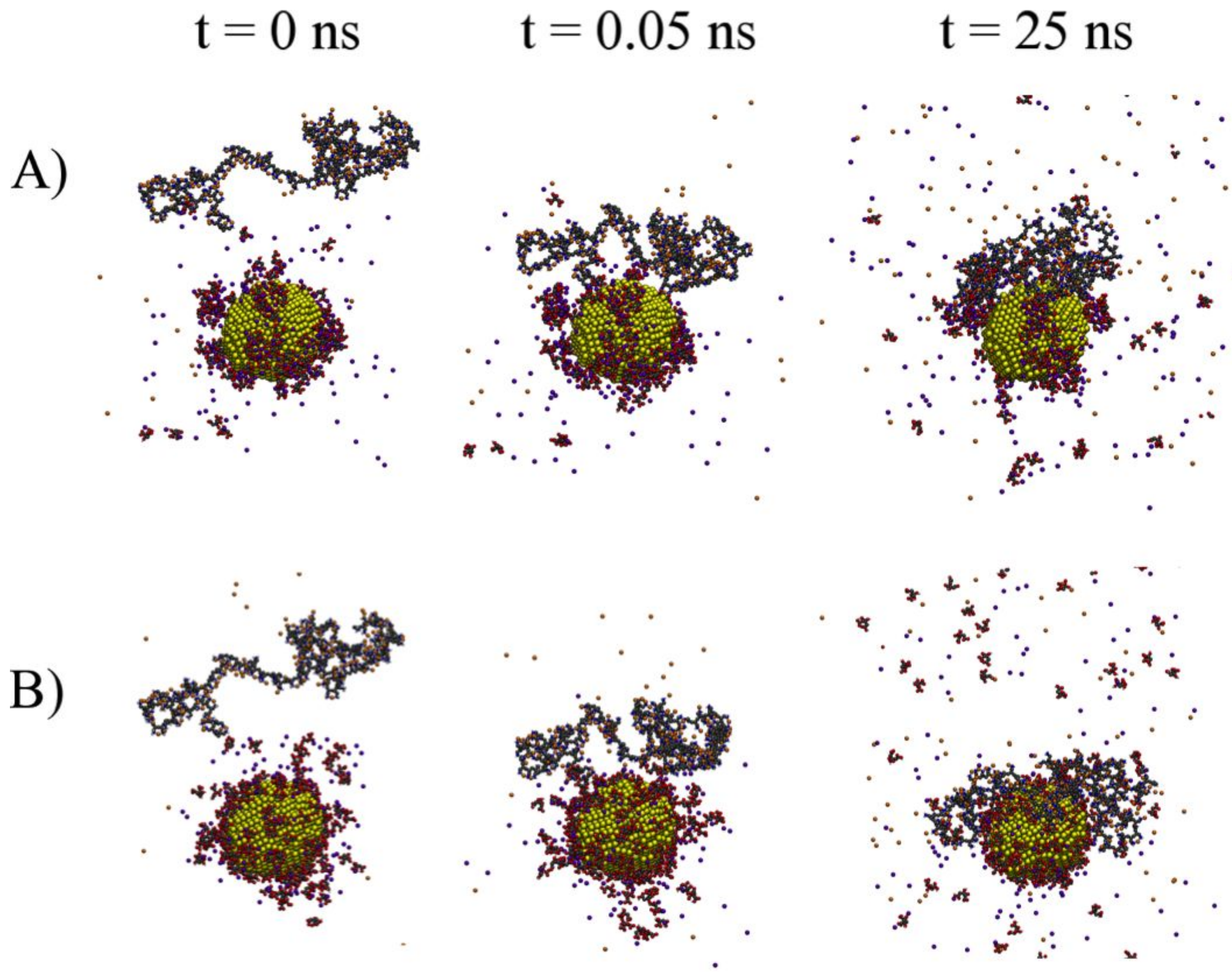

Figure 5. Simulation snapshots of (A) citrate^{3-} and (B) H_2citrate^{-} layers on 4 nm AuNPs in the presence of PAH at the initial configuration (0 ns), after steering PAH to the AuNP surface (0.05 ns), and at the end of equilibration and production runs (25 ns). Gold (yellow), carbon (gray), oxygen (red), hydrogen (white), nitrogen (blue), sodium (purple), and chloride (orange) atoms are shown. Water molecules are not shown for clarity.

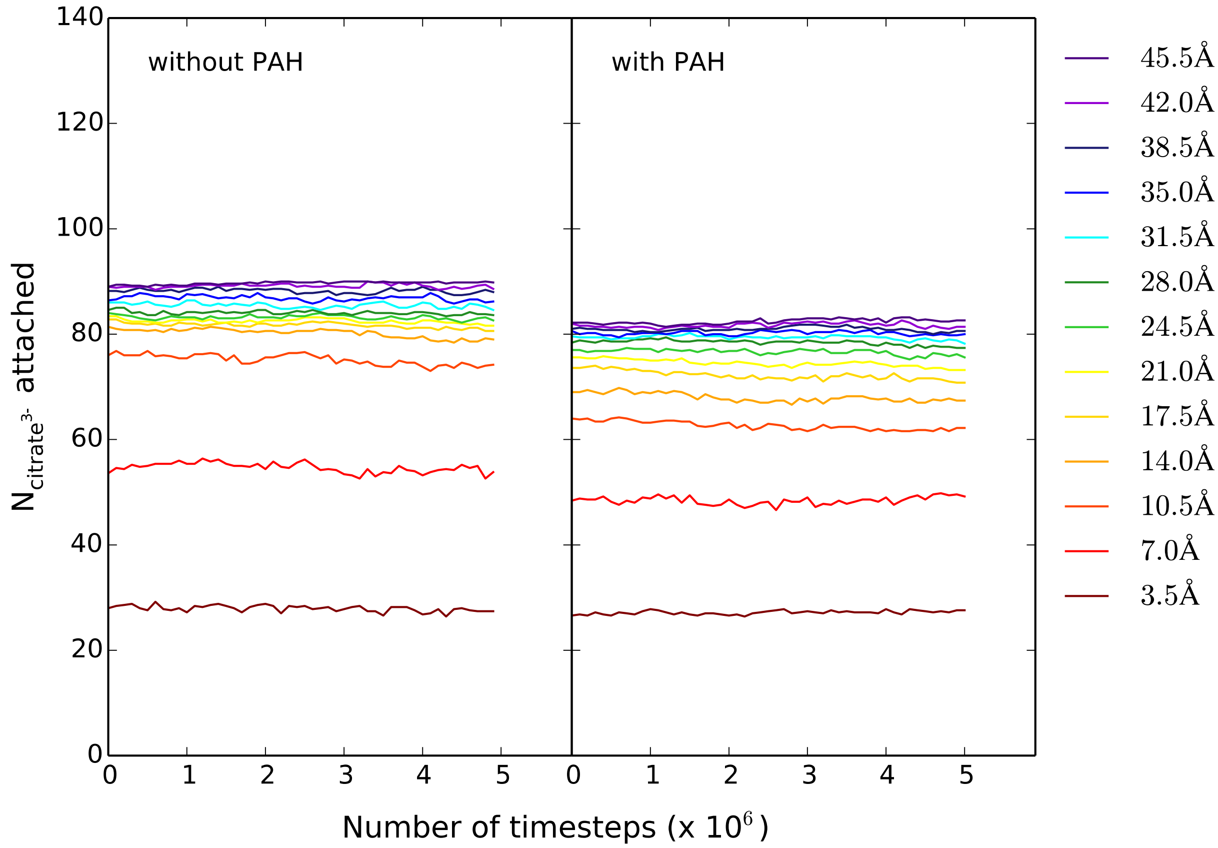

Figure 6. Number of citrate^{3-} within 3.5 Å incremental distances from the 4 nm AuNP surface vs. time in explicit solvent without and with PAH adsorbed. Each curve is an average of five trajectories. There are 27.9 $\pm$ 2.6 citrate directly bound to the surface on 4 nm citrate-coated AuNPs. Beyond 17.5 Å, there is no significant change in the number of citrate between 3.5 Å increments, and free citrate are included in the count. There are 81.7 $\pm$ 2.9 citrate within 17.5 Å of the AuNP surface. The number of surface-bound citrate^{3-} is consistent at 27.2 $\pm$ 4.0 molecules near the AuNP surface, but overall number and spatial distribution of citrate^{3-} near the surface decrease upon adsorption of PAH.

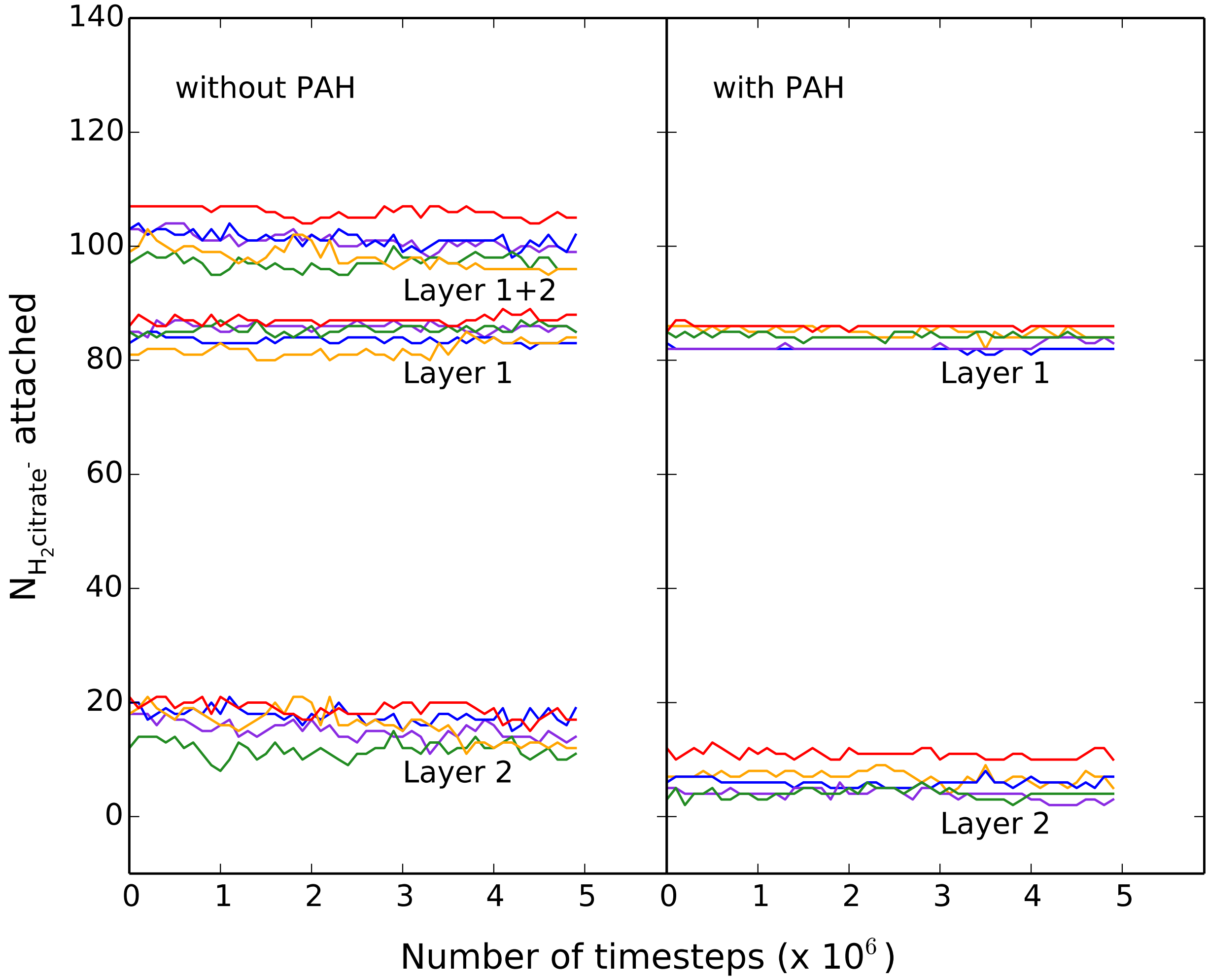

Figure 7. Number of $H_2citrate^-$ in the surface-bound layer (Layer 1), dangling second layer (Layer 2), and the total bilayer (Layer 1+2) on 4 nm AuNPs vs. time in explicit solvent without and with PAH adsorbed. Trajectories are distinguished by color with no association between like colors in different panels. The number of $H_2citrate^-$ in Layer 1 is 84.7 $\pm$ 2.1 without PAH and 83.9 $\pm$ 1.7 $H_2citrate^-$ with PAH adsorbed. The total number of $H_2citrate^-$ in the bilayer on 4 nm AuNPs is 100.7 $\pm$ 3.3 without PAH and 90.3 $\pm$ 3.9 $H_2citrate^-$ with PAH adsorbed.

3.4. Molecular Configurations of Citrate^{3-} and $H_2citrate^-$ on 4 nm Cit-AuNPs and PAH-Cit-AuNPs. The distribution of citrate^{3-} configurations on gold differs between implicit and explicit solvents, but the distribution of $H_2citrate^-$ is in agreement between the solvent conditions (Figures 4 and 8). The different distribution of citrate^{3-} configurations between implicit and explicit solvent is attributed to differences in structure observed between solvent conditions.

Comparison of the distribution of molecular configurations between $citrate^{3-}$ and $H_2citrate^{-}$ in explicit solvent suggests that the tall configurations[16] previously reported to be on 4 nm cit-AuNPs based on ^{13}C SSNMR indicate the presence of either $citrate^{-}$ or $H_2citrate^{-}$, but larger contribution by $H_2citrate^{-}$. The bridge configurations[16] are exclusive to and indicate the presence of $H_2citrate^{-}$ (Figure 8). The oxygen atoms in the central carboxylate and hydroxyl groups of citrate are solvent-exposed in the tall and bridge configurations. Of the 0-, 1-, and 2-arm configurations observed in the simulations, we determined whether a central-carboxylate oxygen, the central-hydroxyl oxygen, or both are bound to the AuNP surface. We find that all hydroxyl oxygen in $citrate^{3-}$ are bound to the surface, exposing the carboxylate groups to solvent to coordinate with Na^{+} ions and that a small percentage of the hydroxyl oxygen in $H_2citrate^{-}$ are free (Figure S6). These configurations are in agreement with previous simulations of $citrate^{3-}$ adlayers on an Au(111) surface[43] and with ATR-FTIR experiments, which found that the hydroxyl group is free below pH 9, and that $citrate^{3-}$ binds to the AuNP surface via both hydroxyl and carboxylate groups above pH 11.[14]

Upon adsorption of PAH, we observe a decrease in the surface-bound layer of the least stable $citrate^{3-}$ configurations—tall and 0-arm—which only have one carboxylate or hydroxyl group bound. For $H_2citrate^{-}$, there is a slight decrease in bridge, tall, and 1-arm configurations and an increase in 2-arm configurations. The intermolecular hydrogen bonding between 2-arm $H_2citrate^{-}$ configurations stabilizes not only the adsorbed citrate anions within the citrate layer but also the interface between the citrate monolayer and adsorbing cationic molecules.

We performed *in situ* ATR-FTIR on multilayered PAH-cit-AuNPs to understand the coordination between citrate within the anionic citrate layer and between the anionic citrate layer and adsorbing polycation layer. Figure 9 shows ATR-FTIR spectra of PAH-cit-AuNPs in solution and after drying. In the region between 3600 and 2800 cm^{-1}, the peak at 3440 cm^{-1} is assigned to the O–H stretching in water clusters that are hydrogen bonded to carboxylic-acid groups.[51] After the sample of PAH-cit-AuNPs is dried, this peak for the water clusters disappears, and the peak at 3385 cm^{-1} is assigned to N–H stretching in PAH.[52] The small peaks at 3041 and 2600 cm^{-1} indicate O–H stretching between hydrogen bonded carboxylic-acid groups,[14,53] which shift slightly after drying the sample. The peak at 2937 cm^{-1} suggests either O–H stretching from the carboxylic-acid group in citrate or a C–H stretch.[53]

In the fingerprint region, characteristic peaks at 1734 cm^{-1} and 1704 cm^{-1} for carbonyl stretches in carboxylic-acid dimers were isolated by Park and Shumaker-Parry[14] after sealing surface-bound $H_2citrate^-$ hydrogen bonded to a dangling $H_2citrate^-$ using long-chain alkanethiols. Our simulations show that the dangling $H_2citrate^-$ layer is displaced upon adsorption of PAH and, thus, this peak is not observed in our FTIR spectra of PAH-cit-AuNPs. The peaks between 1277-1261 cm^{-1} are assigned to C–OH stretching in the carboxylic-acid group of $H_2citrate^-$.[53-54] The peak at 1614 cm^{-1} that shifts to 1603 cm^{-1} in the dried sample is assigned to ν(C=OO⁻) from a salt-bridge formation between a carboxylate group in citrate and NH_3^+ group from PAH, as was previously observed in FTIR spectra of the amino acid glycine ($NH_3^+CH_2COO^-$).[53] These peak assignments are in agreement with simulations showing that 40% of $H_2citrate^-$ on the AuNP surface are in the bridge configuration with terminal carboxylic-acid groups bound to the surface, leaving the central carboxylate group free to interact with PAH (Figure 8). ATR-FTIR experiments combined with molecular dynamics simulations on multilayered PAH-citrate-coated AuNPs further show the importance of $H_2citrate^-$, particularly the bridge configuration, in stabilizing the citrate layer via hydrogen bonding of terminal carboxylic-acid groups and the interface between the citrate layer and adsorbing polycation via salt-bridge formation between the central carboxylate group of citrate and amine group of PAH. This analysis on the coordination of the polycation PAH with amine terminal groups can be broadly applied to study association of protein coronas on cit-AuNPs.

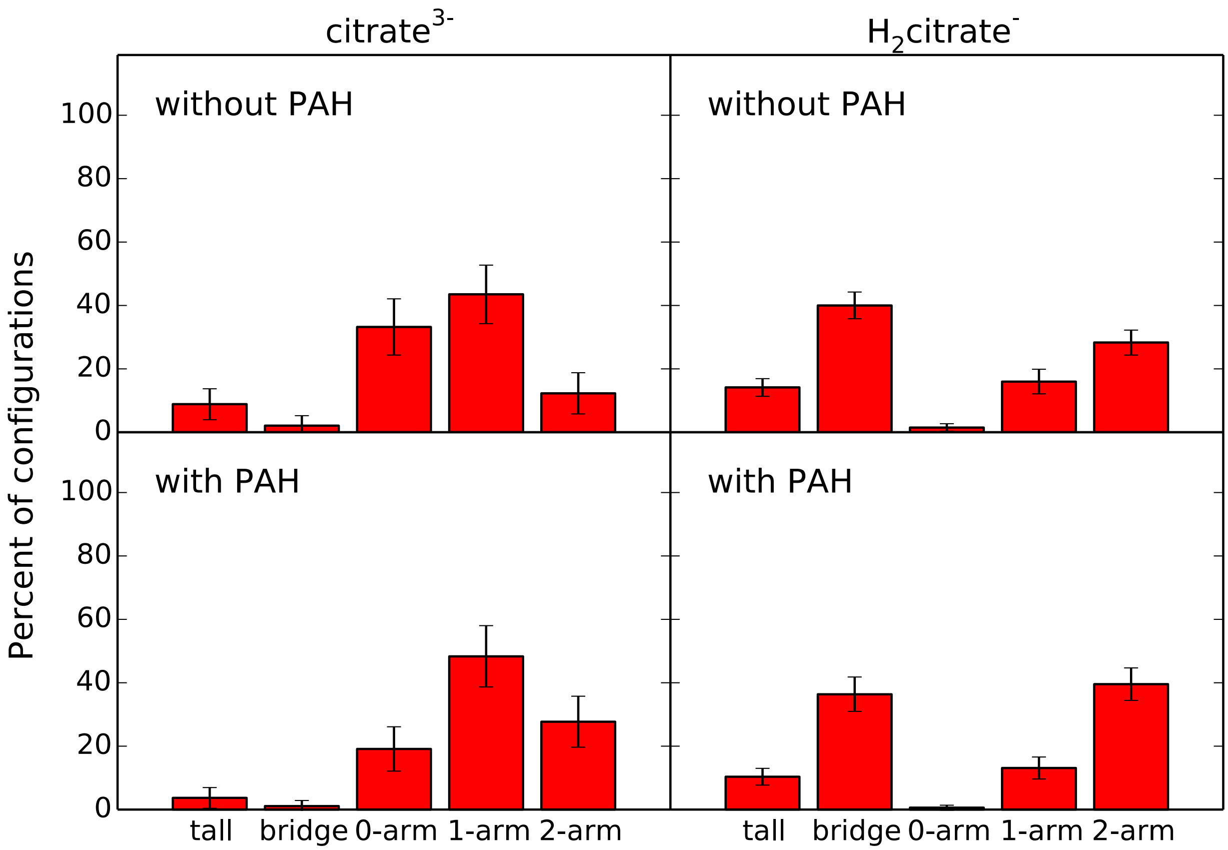

Figure 8. Distribution of molecular configurations in surface-bound citrate^{3-} and H_2citrate^{-} on 4 nm AuNPs in explicit solvent without and with PAH adsorbed.

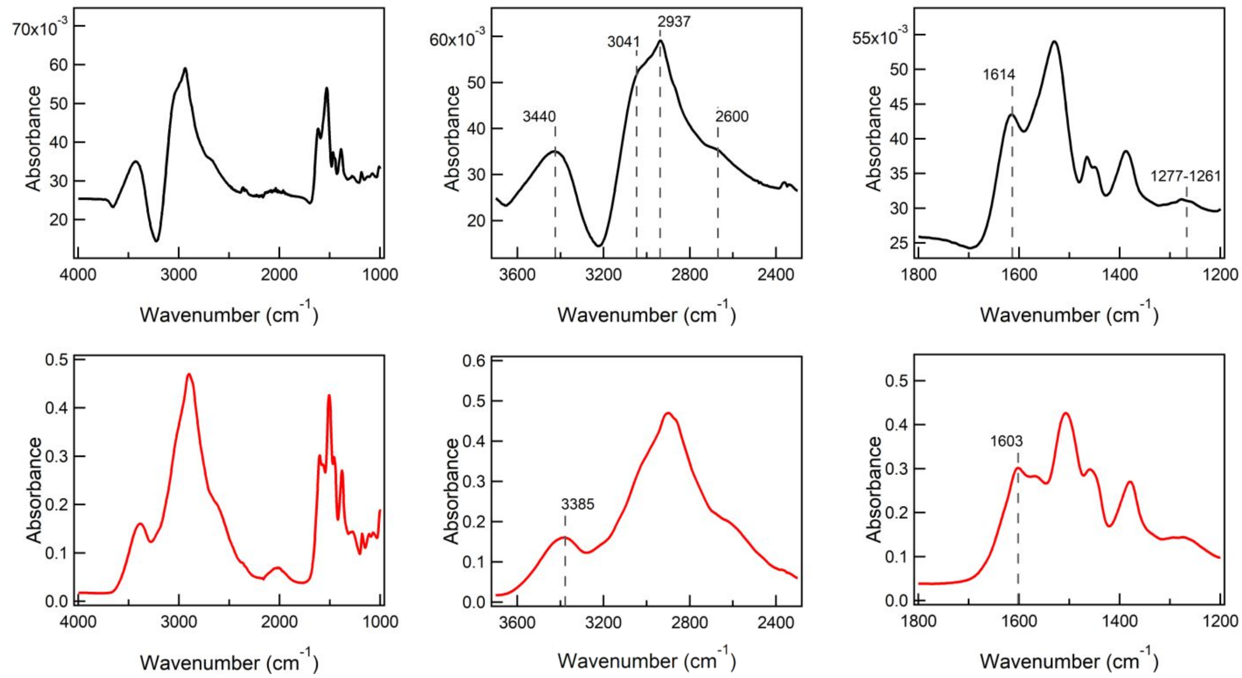

Figure 9. The ATR-FTIR spectrum of PAH-cit-AuNPs in solution (top row) and dry (bottom row): The full (from 4000 cm^{-1} to 1000 cm^{-1}), OH region (from 3700 cm^{-1} to 2300 cm^{-1}) and fingerprint region (from 1800 cm^{-1} to 1200 cm^{-1}) spectra are shown from left to right.

4. Conclusion

We characterize the structure, stability, and density of $citrate^{3-}$ and $H_2citrate^{-}$ on AuNPs, using molecular dynamics simulations. For structure, we find the distribution of tall, bridge, and 2-arm configurations, which are analogous to binding modes of citrate reported in the literature.[14,16] Through implicit-solvent simulations, we confirm that the population of tall configurations increases with increasing packing density[16] and that the distribution of configurations sampled and packing density are independent of AuNP size. Both $citrate^{3-}$ and $H_2citrate^{-}$ can be in the tall configuration, as shown in explicit solvent, but this configuration is more significantly adopted by $H_2citrate^{-}$. For $citrate^{3-}$, the tall configuration can serve to maximize charge separation at high surface charge density. For $H_2citrate^{-}$, the tall configuration maximizes packing, stabilizes the monolayer, and promotes bilayer formation. We find that the bridge configuration is only adopted by H_2citrate$^-$ and suggest its significance is in stabilizing the monolayer and increasing packing. There is a significant presence of the 2-arm configuration compared to other configurations for H_2citrate$^-$ in agreement with previous ATR-FTIR experiments,[14] as the terminal carboxylic-acid groups of H_2citrate$^-$ in this configuration participate in intermolecular hydrogen bonding to stabilize the AuNP surface. However, there is a greater cumulative distribution of 1-arm, tall, and bridge configurations that maximizes packing, thereby yielding a greater density than previously predicted.[14]

We use a combination of molecular dynamics simulations and *in situ* ATR-FTIR experiments to characterize the citrate layer of 4 nm PAH-cit-AuNPs. ATR-FTIR experiments confirm the presence of H_2citrate$^-$ within PAH-cit-AuNPs and agree with configurations between citrate molecules and between citrate and PAH predicted by simulations. We find that the H_2citrate$^-$ layer is highly stable upon PAH adsorption in simulations. In particular, there is a high population of bridge configurations that enables intermolecular hydrogen bonding between citrate via terminal carboxylic-acid groups and salt-bridge formation between the free central carboxylate group in citrate and the amine group in PAH. In contrast, the citrate^{3-} layer is disrupted, and removal of citrate^{3-} from the AuNP surface is observed in the presence of an adsorbing cationic molecule, highlighting the differences in the stability of citrate^{3-} and H_2citrate$^-$ layers, particularly at charged interfaces. The similarity of the distributions between H_2citrate$^-$ and citrate^{3-} configurations across AuNP sizes in implicit solvent, of the distributions of H_2citrate$^-$ configurations between implicit and explicit solvent conditions, and in the structure of citrate^{3-} layers on 4 nm AuNPs and on planar Au(111) surfaces[43] suggests similar structure of citrate layers in larger sized nanoparticles and local response to adsorbing charged molecules at the site of adsorption. For larger sized nanoparticles, the adsorption of multiple polycations or protein coronas must also be considered, and we obtained an all-atom structure for the H_2citrate$^-$ layer and charge density useful for bottom-up coarse-graining simulations of these larger-scale systems.

We determine the density of citrate^{3-} on the AuNP surface to be 2.7×10^{-10} mol/cm^2 and the surface charge density to be 8.1×10^{-10} mol *e*/cm^2, spatially distributed across 17.5 Å radially from the AuNP surface. However, this spatial charge distribution fluctuates upon adsorption of charged molecules. We determine the density of bilayered H_2citrate$^-$ to be 3.3×10^{-10} mol/cm^2. Upon PAH adsorption, the density of monolayered H_2citrate$^-$ remains consistent at 2.8×10^{-10} mol/cm^2 with H_2citrate$^-$ distributed nonuniformly in a face-dependent manner, and total density and surface charge density decreases to 3.0×10^{-10} mol/cm^2 and 3.0×10^{-10} mol *e*/cm^2, respectively, due to some displacement of the dangling, second H_2citrate$^-$ layer by PAH. These values of citrate density and surface charge density are significantly lower than predicted from experimental characterization in dried samples of cit-AuNPs.[9,13] The stability of H_2citrate$^-$ layers justifies the use of fixed-charge models for the representation of the citrate layer in simulations. This also provides an all-atom level determination of the distribution of configurations and coordination modes of citrate predicted by experiment in as-synthesized, functionalized, and transformed cit-AuNPs.

ASSOCIATED CONTENT

Supporting Information. Computational and experimental methods, force-field parameters and additional simulation details, simulation snapshots, and additional figures for the synthesis and characterization of nanoparticles. This material is available free of charge via the Internet at http://pubs.acs.org.

AUTHOR INFORMATION

Corresponding Author

*E-mail: r.hernandez@jhu.edu

ACKNOWLEDGMENTS

This work was supported by National Science Foundation under the Center for Sustainable Nanotechnology (CSN), CHE-1503408. The CSN is part of the Centers for Chemical Innovation Program. E.D.L. acknowledges support by National Science Foundation Graduate Research Fellowship under DGE-1256259. Computing resources were provided in part by the National Science Foundation through XSEDE resources under grant number CTS090079 and by the Maryland Advanced Research Computing Center.

REFERENCES

(1) Turkevich, J.; Stevenson, P. C.; Hillier, J. A Study of the Nucleation and Growth Processes in the Synthesis of Colloidal Gold. *Discuss. Faraday Soc.* **1951,** *11*, 55-75.
(2) Kimling, J.; Maier, M.; Okenve, B.; Kotaidis, V.; Ballot, H.; Plech, A. Turkevich Method for Gold Nanoparticle Synthesis Revisited. *J. Phys. Chem. B* **2006,** *110*, 15700-15707.
(3) Dreaden, E. C.; Alkilany, A. M.; Huang, X.; Murphy, C. J.; El-Sayed, M. A. The Golden Age: Gold Nanoparticles for Biomedicine. *Chem. Soc. Rev.* **2012,** *41*, 2740-2779.
(4) Yang, X.; Yang, M.; Pang, B.; Vara, M.; Xia, Y. Gold Nanomaterials at Work in Biomedicine. *Chem. Rev.* **2015,** *115*, 10410-10488.
(5) Love, J. C.; Estroff, L. A.; Kriebel, J. K.; Nuzzo, R. G.; Whitesides, G. M. Self-Assembled Monolayers of Thiolates on Metals as a Form of Nanotechnology. *Chem. Rev.* **2005,** *105*, 1103-1169.
(6) Vericat, C.; Vela, M. E.; Benitez, G.; Carro, P.; Salvarezza, R. C. Self-Assembled Monolayers of Thiols and Dithiols on Gold: New Challenges for a Well-Known System. *Chem. Soc. Rev.* **2010,** *39*, 1805-1834.
(7) Park, J.-W.; Shumaker-Parry, J. S. Strong Resistance of Citrate Anions on Metal Nanoparticles to Desorption under Thiol Functionalization. *ACS Nano* **2015,** *9*, 1665-1682.
(8) Gole, A.; Murphy, C. J. Polyelectrolyte-Coated Gold Nanorods: Synthesis, Characterization and Immobilization. *Chem. Mater.* **2005,** *17*, 1325-1330.

(9) Dominguez, G. A.; Lohse, S. E.; Torelli, M. D.; Murphy, C. J.; Hamers, R. J.; Orr, G.; Klaper, R. D. Effects of Charge and Surface Ligand Properties of Nanoparticles on Oxidative Stress and Gene Expression within the Gut of *Daphnia magna*. *Aquat. Toxicol.* **2015,** *162*, 1-9.
(10) Falagan-Lotsch, P.; Grzincic, E. M.; Murphy, C. J. One Low-Dose Exposure of Gold Nanoparticles Induces Long-Term Changes in Human Cells. *Proc. Natl. Acad. Sci. U.S.A.* **2016,** *113*, 13318-13323.
(11) Maurer-Jones, M. A.; Gunsolus, I. L.; Murphy, C. J.; Haynes, C. L. Toxicity of Engineered Nanoparticles in the Environment. *Anal. Chem.* **2013,** *85*, 3036-3049.
(12) Murphy, C. J.; Vartanian, A. M.; Geiger, F. M.; Hamers, R. J.; Pedersen, J. A.; Cui, Q.; Haynes, C. L.; Carlson, E. E.; Hernandez, R.; Klaper, R. D., et al. Biological Responses to Engineered Nanomaterials: Needs for the Next Decade. *ACS Cent. Sci.* **2015,** *1*, 117–123.
(13) Rostek, A.; Mahl, D.; Epple, M. Chemical Composition of Surface-Functionalized Gold Nanoparticles. *J. Nanoparticle Res.* **2011,** *13*, 4809-4814.
(14) Park, J.-W.; Shumaker-Parry, J. S. Structural Study of Citrate Layers on Gold Nanoparticles: Role of Intermolecular Interactions in Stabilizing Nanoparticles. *J. Am. Chem. Soc.* **2014,** *136*, 1907-1921.
(15) Torelli, M. D.; Putans, R. A.; Tan, Y.; Lohse, S. E.; Murphy, C. J.; Hamers, R. J. Quantitative Determination of Ligand Densities on Nanomaterials by X-Ray Photoelectron Spectroscopy. *ACS Appl. Mater. Interfaces* **2015,** *7*, 1720-1725.
(16) Al-Johani, H.; Abou-Hamad, E.; Jedidi, A.; Widdifield, C. M.; Viger-Gravel, J.; Sangaru, S. S.; Gajan, D.; Anjum, D. H.; Ould-Chikh, S.; Hedhili, M. N., et al. The Structure and Binding Mode of Citrate in the Stabilization of Gold Nanoparticles. *Nat. Chem.* **2017,** *9*, 890-895.
(17) Girón, J. V. M.; Vico, R. V.; Maggio, B.; Zelaya, E.; Rubert, A.; Benitez, G.; Carro, P.; Salvarezza, R. C.; Vela, M. E. Role of the Capping Agent in the Interaction of Hydrophilic Ag Nanoparticles with DMPC as a Model Biomembrane. *Environ. Sci.: Nano* **2016,** *3*, 462-472.
(18) Gisbert-González, J. M.; Feliu, J. M.; Ferre-Vilaplana, A.; Herrero, E. Why Citrate Shapes Tetrahedral and Octahedral Colloidal Platinum Nanoparticles in Water. *J. Phys. Chem. C* **2018,** *122*, 19004-19014.
(19) Mpourmpakis, G.; Vlachos, D. G. Insights into the Early Stages of Metal Nanoparticle Formation via First-Principle Calculations: The Roles of Citrate and Water. *Langmuir* **2008,** *24*, 7465-7473.
(20) Monti, S.; Barcaro, G.; Sementa, L.; Carravetta, V.; Ågren, H. Characterization of the Adsorption Dynamics of Trisodium Citrate on Gold in Water Solution. *RSC Adv.* **2017,** *7*, 49655-49663.
(21) Murphy, C. J.; Buriak, J. M. Best Practices for the Reporting of Colloidal Inorganic Nanomaterials. *Chem. Mater.* **2015,** *27*, 4911-4913.
(22) Brewer, S. H.; Glomm, W. R.; Johnson, M. C.; Knag, M. K.; Franzen, S. Probing BSA Binding to Citrate-Coated Gold Nanoparticles and Surfaces. *Langmuir* **2005,** *21*, 9303-9307.
(23) Lacerda, S. H. D. P.; Park, J. J.; Meuse, C.; Pristinski, D.; Becker, M. L.; Karim, A.; Douglas, J. F. Interaction of Gold Nanoparticles with Common Human Blood Proteins. *ACS Nano* **2010,** *4*, 365-379.
(24) Casals, E.; Pfaller, T.; Duschl, A.; Oostingh, G. J.; Puntes, V. Time Evolution of the Nanoparticle Protein Corona. *ACS Nano* **2010,** *4*, 3623-3632.
(25) Maiorano, G.; Sabella, S.; Sorce, B.; Brunetti, V.; Malvindi, M. A.; Cingolani, R.; Pompa, P. P. Effects of Cell Culture Media on the Dynamic Formation of Protein-Nanoparticle Complexes and Influence on the Cellular Response. *ACS Nano* **2010,** *4*, 7481-7491.

(26) Goodman, C. M.; McCusker, C. D.; Yilmaz, T.; Rotello, V. M. Toxicity of Gold Nanoparticles Functionalized with Cationic and Anionic Side Chains. *Bioconjugate Chem.* **2004,** *15*, 897-900.
(27) Arvizo, R. R.; Miranda, O. R.; Thompson, M. A.; Pabelick, C. M.; Bhattacharya, R.; Robertson, J. D.; Rotello, V. M.; Prakash, Y. S.; Mukherjee, P. Effect of Nanoparticle Surface Charge at the Plasma Membrane and Beyond. *Nano Lett.* **2010,** *10*, 2543-2548.
(28) Nel, A. E.; Mädler, L.; Velegol, D.; Xia, T.; Hoek, E. M. V.; Somasundaran, P.; Klaessig, F.; Castranova, V.; Thompson, M. Understanding Biophysicochemical Interactions at the Nano-Bio Interface. *Nat. Mater.* **2009,** *8*, 543-557.
(29) Gagner, J. E.; Shrivastava, S.; Qian, X.; Dordick, J. S.; Siegel, R. W. Engineering Nanomaterials for Biomedical Applications Requires Understanding the Nano-Bio Interface: A Perspective. *J. Phys. Chem. Lett.* **2012,** *3*, 3149-3158.
(30) Kim, S. T.; Saha, K.; Kim, C.; Rotello, V. M. The Role of Surface Functionality in Determining Nanoparticle Cytotoxicity. *Acc. Chem. Res.* **2013,** *46*, 681-691.
(31) Pelaz, B.; Charron, G.; Pfeiffer, C.; Zhao, Y.; de la Fuente, J. M.; Liang, X.-J.; Parak, W. J.; del Pino, P. Interfacing Engineered Nanoparticles with Biological Systems: Anticipating Adverse Nano-Bio Interactions. *Small* **2013,** *9*, 1573-1584.
(32) Cui, Q.; Hernandez, R.; Mason, S. E.; Frauenheim, T.; Pedersen, J. A.; Geiger, F. Sustainable Nanotechnology: Opportunities and Challenges for Theoretical/Computational Studies. *J. Phys. Chem. B* **2016,** *120*, 7297-7306.
(33) Zhu, G.; Huang, Z.; Xu, Z.; Yan, L.-T. Tailoring Interfacial Nanoparticle Organization through Entropy. *Acc. Chem. Res.* **2018,** *51*, 900-909.
(34) Chong, G.; Hernandez, R. Adsorption Dynamics and Structure of Polycations on Citrate-Coated Gold Nanoparticles. *J. Phys. Chem. C* **2018,** *122*, 19962-19969.
(35) Olenick, L. L.; Troiano, J. M.; Vartanian, A. M.; Melby, E. S.; Mensch, A. C.; Zhang, L.; Hong, J.; Qiu, T. A.; Bozich, J. S.; Lohse, S. E., et al. Lipid Corona Formation from Nanoparticle Interactions with Bilayers *Chem* **2018,** *4*, 2709-2723.
(36) Lin, W.; Insley, T.; Tuttle, M. D.; Zhu, L. Y.; Berthold, D. A.; Kral, P.; Rienstra, C. M.; Murphy, C. J. Control of Protein Orientation on Gold Nanoparticles. *J. Phys. Chem. C* **2015,** *119*, 21035-21043.
(37) Brancolini, G.; Corazza, A.; Vuano, M.; Fogolari, F.; Mimmi, M. C.; Bellotti, V.; Stoppini, M.; Corni, S.; Esposito, G. Probing the Influence of Citrate-Capped Gold Nanoparticles on an Amyloidogenic Protein. *ACS Nano* **2015,** *9*, 2600-2613.
(38) Ramalho, J. P. P.; Gkeka, P.; Sarkisov, L. Structure and Phase Transformations of DPPC Lipid Bilayers in the Presence of Nanoparticles: Insights from Coarse-Grained Molecular Dynamics Simulations. *Langmuir* **2011,** *27*, 3723-3730.
(39) Li, Y.; Zhang, X.; Cao, D. Self-Assembly of Patterned Nanoparticles on Cellular Membranes: Effect of Charge Distribution. *J. Phys. Chem. B* **2013,** *117*, 6733-6740.
(40) Chen, P.; Huang, Z.; Liang, J.; Cui, T.; Zhang, X.; Miao, B.; Yan, L.-T. Diffusion and Directionality of Charged Nanoparticles on Lipid Bilayer Membrane. *ACS Nano* **2016,** *10*, 11541-11547.
(41) Rossi, G.; Monticelli, L. Gold Nanoparticles in Model Biological Membranes: A Computational Perspective. *Biochim. Biophys. Acta* **2016,** *1858*, 2380-2389.
(42) Phanchai, W.; Srikulwong, U.; Chompoosor, A.; Sakonsinsiri, C.; Puangmali, T. Insight into the Molecular Mechanisms of AuNP-Based Aptasensor for Colorimetric Detection: A Molecular Dynamics Approach. *Langmuir* **2018,** *34*, 6161-6169.

(43) Wright, L. B.; Rodger, P. M.; Walsh, T. R. Structure and Properties of Citrate Overlayers Adsorbed at the Aqueous Au(111) Interface. *Langmuir* **2014,** *30*, 15171-15180.
(44) Mdluli, P. S.; Sosibo, N. M.; Mashazi, P. N.; Nyokong, T.; Tshikhudo, R. T.; Skepu, A.; van der Lingen, E. Selective Adsorption of PVP on the Surface of Silver Nanoparticles: A Molecular Dynamics Study. *J. Mol. Struct.* **2011,** *1004*, 131-137.
(45) Kyrychenko, A.; Korsun, O. M.; Gubin, I. I.; Kovalenko, S. M.; Kalugin, O. N. Atomistic Simulations of Coating of Silver Nanoparticles with Poly(vinylpyrrolidone) Oligomers: Effect of Oligomer Chain Length. *J. Phys. Chem. C* **2015,** *119*, 7888-7899.
(46) Heinz, H.; Farmer, B. L.; Pandey, R. B.; Slocik, J. M.; Patnaik, S. S.; Pachter, R.; Naik, R. R. Nature of Molecular Interactions of Peptides with Gold, Palladium, and Pd-Au Bimetal Surfaces in Aqueous Solution. *J. Am. Chem. Soc.* **2009,** *131*, 9704-9714.
(47) Jha, K. C.; Liu, H.; Bockstaller, M. R.; Heinz, H. Facet Recognition and Molecular Ordering of Ionic Liquids on Metal Surfaces. *J. Phys. Chem. C* **2013,** *117*, 25969-25981.
(48) Plimpton, S. Fast Parallel Algorithms for Short-Range Molecular-Dynamics. *J. Comput. Phys.* **1995,** *117*, 1-19.
(49) Lohse, S. E.; Eller, J. R.; Sivapalan, S. T.; Plews, M. R.; Murphy, C. J. A Simple Millifluidic Benchtop Reactor System for the High-Throughput Synthesis and Functionalization of Gold Nanoparticles with Different Sizes and Shapes. *ACS Nano* **2013,** *7*, 4135-4150.
(50) Jeffrey, G. A., *An Introduction to Hydrogen Bonding*. Oxford University Press: New York, 1997.
(51) Wang, S.; Yao, H.; Sato, S.; Kimura, K. Inclusion-Water-Cluster in a Three-Dimensional Superlattice of Gold Nanoparticles. *J. Am. Chem. Soc.* **2004,** *126*, 7438-7439.
(52) Bossa, J.-B.; Borget, F.; Duvernay, F.; Theulé, P.; Chiavassa, T. Formation of Neutral Methylcarbamic Acid ($CH_3NHCOOH$) and Methylammonium Methylcarbamate $[CH_3NH_3^+][CH_3NHCO_2^-]$ at Low Temperature. *J. Phys. Chem. A* **2008,** *112*, 5113-5120.
(53) Max, J.-J.; Chapados, C. Infrared Spectroscopy of Aqueous Carboxylic Acids: Comparison between Different Acids and their Salts. *J. Phys. Chem. A* **2004,** *108*, 3324-3337.
(54) Mudunkotuwa, I. A.; Grassian, V. H. Citric Acid Adsorption on TiO_2 Nanoparticles in Aqueous Suspensions at Acidic and Circumneutral pH: Surface Coverage, Surface Speciation, and Its Impact on Nanoparticle-Nanoparticle Interactions. *J. Am. Chem. Soc.* **2010,** *132*, 14986-14994.

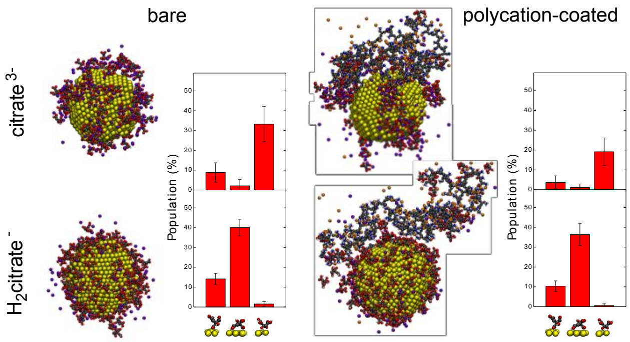
bare
polycation-coated
citrate 3-
H2citrate -
Population (%)
Population (%)

TOC Graphic